

COMPREHENSIVE ANALYSIS OF PREBIOTIC PROPENAL UP TO 660 GHz

A. M. DALY^{1,2}, C. BERMÚDEZ¹, L. KOLESNIKOVA¹, AND J. L. ALONSO¹

¹ Grupo de Espectroscopia Molecular (GEM), Edificio Quifima, Área de Química-Física, Laboratorios de Espectroscopia y Bioespectroscopia, Parque Científico UVa, Unidad Asociada CSIC, Universidad de Valladolid, E-47011 Valladolid, Spain; Adam.M.Daly@jpl.nasa.gov

² Jet Propulsion Laboratory, California Institute of Technology, 4800 Oak Grove Dr., Pasadena, CA 91109, USA

Received 2015 March 13; accepted 2015 May 8; published 2015 June 22

ABSTRACT

Since interstellar detection of propenal is only based on two rotational transitions in the centimeter wave region, its high resolution rotational spectrum has been measured up to 660 GHz and fully characterized by assignment of more than 12,000 transitions to provide direct laboratory data to the astronomical community. Spectral assignments and analysis include transitions from the ground state of the *trans* and *cis* isomers, three *trans*-¹³C isotopologues, and ten excited vibrational states of the *trans* form. Combining new millimeter and submillimeter data with those from the far-infrared region has yielded the most precise set of spectroscopic constants of *trans*-propenal obtained to date. Newly determined rotational constants, centrifugal distortion constants, vibrational energies, and Coriolis and Fermi interaction constants are given with high accuracy and were used to predict transition frequencies and intensities over a wide frequency range. Results of this work should facilitate astronomers further observation of propenal in the interstellar medium.

Key words: catalogs – ISM: molecules – molecular data – techniques: spectroscopic

Supporting material: machine-readable tables

1. INTRODUCTION

Ever since the discovery of the simplest aldehyde (formaldehyde) in the interstellar medium (ISM), aldehydes have also been called the “sugars of space” (Snyder et al. 1969). Detection of these “sugars of space” is associated mainly to molecular clouds, which may indicate that the reactions occurring in grains facilitate their formation (Ikeda et al. 2001). So far, the observation of lines belonging to these aldehydes is restricted to molecules with chains containing no more than three carbon atoms, with propenal (acrolein), CH₂CHCHO, the simplest conjugated aldehyde, being one of the largest. Additionally, propenal is considered to be a prebiotic molecule owing both to its formation in the decomposition of sugars (Moldoveanu 2010; Bermúdez et al. 2013) and its implication in the synthesis of amino acids, such as methionine and glutamic acid, via Strecker-type reactions (van Trump & Miller 1972). Its generation in the ISM has been postulated to be a product of a simple hydrogen addition reaction from a known interstellar aldehyde, propynal (Irvine et al. 1988; Turner 1991). Nevertheless, while more than 40 transitions have been found belonging to other relevant aldehydes, such as glycolaldehyde, in different regions of the ISM (Hollis et al. 2000; Halfen et al. 2006; Beltrán et al. 2009; Jørgensen et al. 2012), positive detection of propenal has thus far been based on only two transitions of its lower energy *trans* isomer in the ground vibrational state, namely 2₁₁ ← 1₁₀ and the 3₁₃ ← 2₁₂ at 18221.164 (2) and 26079.449 (1) MHz, respectively, observed by the 100 m Green Bank Telescope pointing toward the star-forming region of Sagittarius B2(N) (Hollis et al. 2004; Requena-Torres et al. 2008). With the increasing sensitivity of astrophysical detection facilities, it might now be possible to identify not only further lines of *trans*-propenal, but also transitions from ¹³C isotopologues, excited vibrational states, or the higher energy *cis* isomeric form. The key to success in this astrophysical identification lies in analyzing propenal pure rotational transitions, especially those that fall into the millimeter- and submillimeter-wave

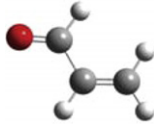
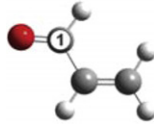
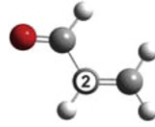
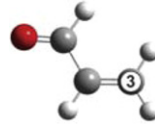
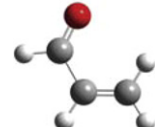
regions, which are the working domains for the IRAM, NRAO, SEST, CSO telescopes, or ALMA interferometers.

Propenal can be observed in two *trans* and *cis* planar C_s conformers that interchange by rotation around the single C–C bond (see figures in Table 1), the *cis* form being 600 cm⁻¹ higher in energy than the *trans* one (Blom & Bauder 1982). Ground state rotational spectra of both conformers, their isotopologues, and the lowest-energy excited vibrational state have already been studied in the microwave region (Fine et al. 1955; Wagner et al. 1957; Cherniak & Costain 1966; Blom & Bauder 1982; Blom et al. 1984). However, apart from the ground vibrational state of *trans*-propenal, which has been analyzed up to 170 GHz (Winnewisser et al. 1975), no further information exists on the rotational spectrum of propenal. Since there is always an uncertainty involved in predicting transitions at higher frequencies, interstellar detection of new propenal lines should be based on transitions measured directly in the laboratory or transitions predicted from a data set that includes higher frequency lines. In the present work, the pure rotational spectrum of propenal up to 660 GHz has been analyzed for the ground vibrational state of *cis*- and *trans*-propenal, the three ¹³C isotopologues of the latter and ten lowest energy excited vibrational states below 700 cm⁻¹. Given the strong Coriolis and Fermi perturbations observed, a global fit analysis combining our pure rotational and previously published vibrational rotational data (McKellar et al. 2007; McKellar & Appadoo 2008) was required. A highly accurate set of spectroscopic parameters that reproduce the spectrum and can facilitate detections of propenal in the ISM was thus obtained.

2. EXPERIMENTAL DETAILS

A commercially available sample of liquid propenal (b.p. = 125 °C) was used without further purification. Propenal spectrum was acquired using two different spectrometers. A recently upgraded Stark-modulation spectrometer employing 33 kHz modulation frequency and phase-sensitive detection (J. L. Alonso et al., in preparation) was used to cover the

Table 1
Ground State Spectroscopic Constants of the *Trans*-propenal Parent and ^{13}C -species and *Cis*-propenal (*A*-reduction, *f*-representation)

Constant	Unit	<i>Trans</i> -propenal	<i>Trans</i> - $^{13}\text{C}_1$	<i>Trans</i> - $^{13}\text{C}_2$	<i>Trans</i> - $^{13}\text{C}_3$	<i>Cis</i> -propenal
...	...					
<i>A</i>	MHz	47353.7074 (17) ^a	46781.0275 (67)	46518.9165 (64)	47255.1934 (73)	22831.6487 (43)
<i>B</i>	MHz	4659.499468 (61)	4644.74135 (19)	4642.43842 (17)	4520.79374 (15)	6241.04728 (35)
<i>C</i>	MHz	4242.689488 (56)	4225.83534 (20)	4221.74338 (19)	4126.64084 (18)	4902.20757 (21)
Δ_J	kHz	1.042067 (19)	1.03970 (10)	1.03172 (10)	0.988410 (65)	5.11335 (24)
Δ_{JK}	kHz	-8.78538 (44)	-8.6890 (24)	-8.7575 (13)	-8.9704 (14)	-29.1854 (13)
Δ_K	kHz	360.363 (64)	348.56 (23)	367.21 (22)	363.31 (26)	108.07 (12)
δ_J	kHz	0.1202675 (76)	0.120817 (20)	0.121459 (18)	0.111595 (18)	1.48116 (12)
δ_K	kHz	5.7481 (24)	5.643 (10)	5.745 (10)	5.441 (10)	11.3386 (76)
Φ_J^b	mHz	0.2994 (25)	0.209 (20)	0.274 (21)	0.287 (11)	1.601 (89)
Φ_{JK}	mHz	-6.576 (46)	-6.576 ^c	-6.576 ^c	-6.576 ^c	92.04 (49)
Φ_{KJ}	mHz	-510.0 (12)	-382 (19)	-536.1 (64)	-459.1 (70)	-1153.0 (21)
ϕ_J	mHz	0.0740 (11)	0.0740 ^c	0.0740 ^c	0.0740 ^c	1.082 (43)
ϕ_{JK}	mHz	5.00 (62)	5.00 ^c	5.00 ^c	5.00 ^c	-19.3 (20)
<i>J</i> range	...	5–73	1–55	1–55	1–67	1–61
<i>K_a</i> range	...	0–19	0–12	0–16	0–16	0–23
$N_{\text{lines}}/N_{\text{ex}}^d$...	1606/28	492/103	531/85	485/93	574/78
σ_{fit}^e	kHz	37	40	40	41	39

Note.

^a The numbers in parentheses are 1σ uncertainties in the units of the last decimal digit.

^b Purely *K*-dependent sextic centrifugal distortion constants Φ_K and ϕ_K could not be determined from the present data sets.

^c Fixed to the parent species value.

^d Number of distinct frequency fitted lines/number of excluded lines based on the $2u$ fitting criterion of the SPFIT program (Pickett 1991) where u is the uncertainty of the measured frequency. The uncertainties between 50 and 500 kHz were given to the millimeter and submillimeter data from this work and 100 kHz to the microwave data from Blom & Bauder (1982), Blom et al. (1984).

^e Standard deviation of the fit.

26–110 GHz range. Millimeter- and submillimeter-wave measurements, over the 50–660 GHz range, were performed using a direct absorption spectrometer recently constructed at the University of Valladolid (Daly et al. 2014). It is based on the frequency multiplier chains (VDI, Inc.) driven by an Agilent E8257D microwave synthesizer. The signal was detected using solid-state zero-bias detectors (VDI, Inc.) at twice the modulation frequency ($2f = 20.4$ kHz) and with a modulation depth between 20 and 50 kHz resulting in the second derivative line shape. All spectra were taken at room temperature with sample pressure less than 30 mTorr and recorded in 1 GHz sections in both directions. Rotational spectra of all three ^{13}C isotopologues were measured in their natural abundances. Transition lines were measured using a Gaussian profile function (AABS package; Kisiel et al. 2005) with accuracy better than 50 kHz for isolated well-developed lines (the accuracy up to 500 kHz was given to lines with poor signal-to-noise ratio).

3. ROTATIONAL SPECTRA AND ANALYSIS

3.1. Ground Vibrational State

The ground state rotational spectrum of *trans*-propenal is dominated by strong *a*-type *R*-branch transitions and weaker *b*-type *R*-branch and *Q*-branch transitions, in agreement with the values of the dipole moment components $|\mu_a| = 3.052$ (4) D and $|\mu_b| = 0.630$ (1) D (Blom et al. 1984). Starting with the predictions based on the previous results and following an iterative process of assignment and fitting, over 1900 lines were

assigned up to $J = 76$ and $K_a = 24$. The following Watson's *A*-reduced semi-rigid Hamiltonian up to the sixth order (Watson 1977) was used in the analysis

$$\begin{aligned}
 H_{\text{Rot}}^{(v)} = & AJ_a^2 + BJ_b^2 + CJ_c^2 - \Delta_J J^4 - \Delta_{JK} J^2 J_a^2 \\
 & - \Delta_K J_a^4 - \frac{1}{2} [\delta_J J^2 + \delta_K J_a^2, J_+^2 + J_-^2]_+ \\
 & + \Phi_J J^6 + \Phi_{JK} J^4 J_a^2 + \Phi_{KJ} J^2 J_a^4 \\
 & + \Phi_K J_a^6 + \frac{1}{2} [\phi_J J^4 + \phi_{JK} J^2 J_a^2 \\
 & + \phi_K J_a^4, J_+^2 + J_-^2]_+
 \end{aligned} \quad (1)$$

where A , B , C are the rotational constants, Δ_J , Δ_{JK} , Δ_K , δ_J , δ_K are quartic, and Φ_J , Φ_{JK} , Φ_{KJ} , Φ_K , ϕ_J , ϕ_{JK} , ϕ_K are sextic centrifugal distortion constants. Some series of high K_a -rotational transitions were found to be perturbed and could not be fitted within the distortable rotor model, hence, they were not included in the current stage of the fit. These perturbations were later treated in the global analysis presented in the following section. The spectroscopic parameters derived are listed in the first column of Table 1.

Around 500 distinct frequency ground state lines for each ^{13}C -species were analyzed in terms of the same Hamiltonian given by Equation (1) with Φ_{JK} , ϕ_J , and ϕ_{JK} constants fixed to the values of the parent species. Since our measurements were performed in natural abundance (intensities about 1% of the parent species), only the intense *a*-type transitions were

Table 2
Laboratory Assigned and Fitted Transition Frequencies for the *Trans*-propenal Parent, *Trans*-¹³C-species, *Cis*-propenal Ground States and Ten Excited Vibrational States of *Trans*-propenal

Species	Transition ^a								ν_{obs}^b (MHz/cm ⁻¹)	$\nu_{\text{obs}} - \nu_{\text{calc}}^c$ (MHz/cm ⁻¹)	Comment ^d	References
	J'	K'_a	K'_c	v'	J''	K''_a	K''_c	v''				
<i>Trans</i> - ¹³ C ₁	16	1	16	0	15	1	15	0	138100.896	0.040	...	(2)
<i>Trans</i> - ¹³ C ₁	16	0	16	0	15	0	15	0	139964.297	0.020	...	(2)
<i>Trans</i> - ¹³ C ₂	20	7	13	0	19	7	12	0	177365.923	-0.031	...	(2)
<i>Trans</i> - ¹³ C ₂	20	6	14	0	19	6	13	0	177394.047	0.053	B	(2)
<i>Trans</i> - ¹³ C ₂	20	6	15	0	19	6	14	0	177394.047	0.056	B	(2)
<i>Trans</i> - ¹³ C ₃	16	0	16	0	15	0	15	0	136624.069	0.005	...	(2)
<i>Trans</i> - ¹³ C ₃	20	1	19	0	19	1	18	0	175805.698	0.121	U	(2)
<i>Cis</i>	17	1	16	0	16	1	15	0	182121.954	-0.030	...	(2)
<i>Cis</i>	16	2	14	0	15	2	13	0	184240.673	-0.006	...	(2)
<i>Trans</i>	23	2	22	0	22	2	21	0	203709.166	-0.031	...	(2)
<i>Trans</i>	23	2	22	3	22	2	21	3	203716.290	0.012	...	(2)
<i>Trans</i>	23	2	22	10	22	2	21	10	203840.124	-0.005	...	(2)

Notes.

^a Upper and lower state quantum numbers are indicated by “and,” respectively. The assignment of the individual vibrational states to v is as following: $0 \rightarrow$ ground state, $1 \rightarrow v_{18} = 1$, $2 \rightarrow v_{18} = 2$, $3 \rightarrow v_{13} = 1$, $4 \rightarrow v_{18} = 3$, $5 \rightarrow (v_{18} = 1, v_{13} = 1)$, $6 \rightarrow v_{12} = 1$, $7 \rightarrow v_{17} = 1$, $8 \rightarrow v_{18} = 4$, $9 \rightarrow (v_{18} = 2, v_{13} = 1)$, and $10 \rightarrow v_{13} = 2$.

^b Observed frequency. Microwave, millimeter and submillimeter data are in MHz while the far-infrared data are in cm⁻¹.

^c Observed minus calculated frequency.

^d Blended transitions were fitted to their intensity weighted averages and are labeled by B. Unfitted transitions are labeled by U.

References. (1) Blom et al. (1984); (2) This work; (3) Blom & Bauder (1982); (4) Winnewisser et al. (1975); (5) McKellar & Appadoo (2008).

(This table is available in its entirety in machine-readable form.)

observed. These transitions were combined with the *a*- and *b*-type ones measured by Blom et al. (1984) using isotopically highly enriched samples. The final sets of the spectroscopic constants are also given in Table 1.

For *cis*-propenal ($|\mu_a| = 2.010(5)$ D and $|\mu_b| = 1.573(3)$ D (Blom & Bauder 1982)), more than 500 lines were assigned to *a*- and *b*-type *R*-branch transitions up to $J = 60$ and $K_a = 23$ and were analyzed using the above-mentioned Hamiltonian. The derived spectroscopic constants are listed in the last column of Table 1. Line assignments, observed frequencies ν_{obs} , $\nu_{\text{obs}} - \nu_{\text{calc}}$ values, where ν_{calc} is the calculated frequency based on the Hamiltonian model used, and references of the data sources included in the final fits for the *trans*-¹³C-species and *cis*-propenal ground states are presented in Table 2.

3.2. Excited Vibrational States

Trans-propenal has four low-lying vibrational modes involving skeletal C–C torsion (ν_{18}), C=C–C bending (ν_{13}), O=C–C bending (ν_{12}), and =CH₂ twisting mode (ν_{17}). Up to 10 vibrational states below 700 cm⁻¹ (see Figure 1) can be sufficiently populated at the room temperature of the experiment to generate a highly rich vibrational satellite spectrum. Stark-modulation microwave spectroscopy is a very useful tool for analyzing these rotational satellite lines as has recently been shown in works on ethyl (Daly et al. 2014) and vinyl cyanide (López et al. 2014). When an electric field is applied to a rotating molecule, the *M*-degeneracy is partially or fully removed. This perturbation of the rotational energy levels by electric field gives rise to a Stark spectrum. A section of the Stark spectrum around the ground state $4_{14} \leftarrow 3_{13}$ rotational transition of *trans*-propenal is presented in Figure 2. Rotational transitions in the excited vibrational states were readily

assigned on the basis of their characteristic Stark patterns (negative lobes in Figure 2), the same as the ground state line. Hence, at the higher frequency side of the ground state line, a harmonic progression formed by four satellite lines can easily be identified and assigned to pure rotational transition in successive excited vibrational states of the ν_{18} torsional mode. Moreover, pure rotational spectra in other excited states corresponding to $\nu_{13} = 1$, $\nu_{12} = 1$, $\nu_{17} = 1$ as well as combination states ($\nu_{18} = 1, \nu_{13} = 1$) and ($\nu_{18} = 2, \nu_{13} = 1$) were also observed. Preliminary spectroscopic constants obtained for these 10 excited states were used to predict the corresponding rotational spectra in the millimeter- and submillimeter-wave region. Loomis–Wood type plots, originally described by Loomis & Wood (1928), from the AABS package (Kisiel et al. 2005, 2012) were used to facilitate identification of rotational transitions for each vibrational state.

During the analysis of propenal in the millimeter and submillimeter region, the major complication is due to the mutual interactions between excited vibrational states belonging to low-lying vibrational modes leading to strong perturbations in the spectrum. The possible interactions between two states depends on the symmetry classification of the states involved which is marked in Figure 1 according to the C_s symmetry point group. Vibrational states belonging to different symmetry species may be connected by *a*- and *b*-type Coriolis interaction terms, and excited states with the same symmetry species may be coupled through *c*-type Coriolis and Fermi interactions. Figure 1 shows how the lowest-energy $\nu_{18} = 1$ excited state should be free of interactions due to its energy spacing with respect to other excited states. Over 1000 pure rotational transitions could be included in the fit using the Equation (1). Nonetheless, several K_a series revealed deviations that could not be taken into account by adding higher-

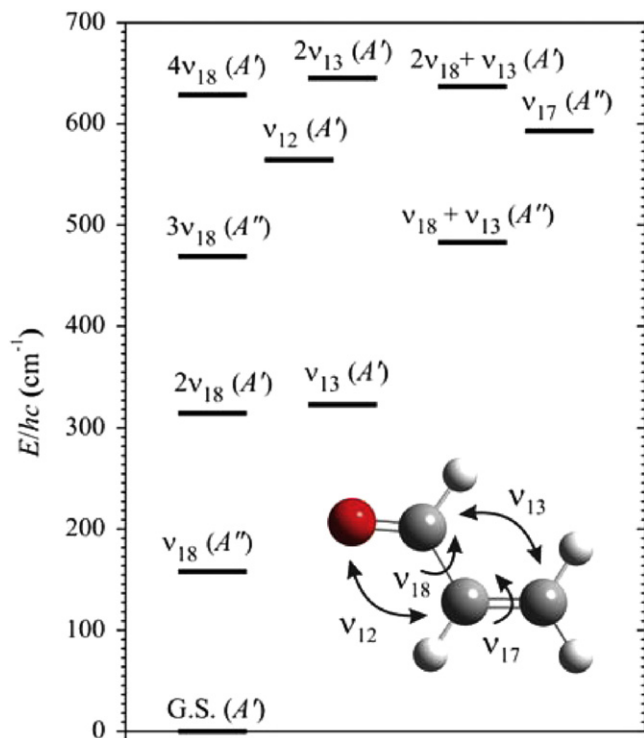


Figure 1. Vibrational energy levels of *trans*-propenal below 700 cm^{-1} obtained by McKellar & Appadoo (2008) and schematic illustration of the four lowest-energy normal vibrational modes, ν_{18} : C–C torsion, ν_{13} : C=C–C bending mode, ν_{12} : O=C–C bending mode, and ν_{17} : CH_2 twisting mode. The symmetry specifications are given in accordance with C_s point group.

order centrifugal distortion effects. Some of these anomalies were observed exactly within the same range of the J quantum numbers as those already observed for ground state transitions. This clearly indicates that the ground state is in mutual interaction with the $\nu_{18} = 1$ excited state and, as a result, they were analyzed together. Even though both a - and b -type Coriolis couplings are allowed in this case, only b -type Coriolis terms were found to be significant in the fitting. Including the Coriolis terms in the analysis improved the fit considerably, although, several K_a series of transitions in $\nu_{18} = 1$ could still not be reproduced. A deeper insight into the $\nu_{18} = 1$ rotational energy levels showed further interactions with higher-energy $\nu_{18} = 2$ state. This significantly complicates the analysis since the $\nu_{18} = 2$ state cannot be analyzed without the neighboring

almost iso-energetic $\nu_{13} = 1$ state due to strong c -type Coriolis and Fermi interactions between them. A close look at the microwave spectrum in Figure 2 shows a small shift of the $\nu_{18} = 2$ transition from the equidistant pattern which reflects the strong coupling between this state and $\nu_{13} = 1$. A 4-state Hamiltonian analysis was thus performed to correctly reproduce all the perturbed transitions in the ground state, $\nu_{18} = 1$, $\nu_{18} = 2$, and $\nu_{13} = 1$ excited vibrational states. Two excited vibrational states, $\nu_{18} = 3$ and $(\nu_{18} = 1, \nu_{13} = 1)$, were then also analyzed as an interacting pair connected through c -type Coriolis and Fermi interactions. Possible interactions of this pair with other states were ignored. Analysis of the five remaining excited vibrational states above 500 cm^{-1} led to the identification of many local perturbations. Although the $\nu_{12} = 1$ and $\nu_{17} = 1$ pair was initially treated separately, a 5-state Hamiltonian including $\nu_{12} = 1$, $\nu_{17} = 1$, $\nu_{18} = 4$, $(\nu_{18} = 2, \nu_{13} = 1)$, and $\nu_{13} = 2$ excited vibrational states was inevitable.

3.3. Global Analysis

Over 10,000 distinct frequency lines treated in the above-mentioned 4-state, 2-state, and 5-state analyses were finally combined with more than 8000 lines available from high resolution vibration-rotation study of McKellar & Appadoo (2008). The uncertainties between 50 and 500 kHz were given to the millimeter and submillimeter data and between 0.0003 and 0.001 cm^{-1} to the far-infrared data for weighing purposes of the nonlinear least-square fit. The Hamiltonian matrix constructed for this problem can be written in standard block form with 11×11 array size. Each diagonal block consists of $H_{\text{Rot}}^{(v)} + \Delta E_v$ term where $H_{\text{Rot}}^{(v)}$ is the Watson's A -reduced rotational Hamiltonian for given vibrational state v defined by Equation (1) and $\Delta E_v = E_v - E_0$ is the vibrational energy difference from the ground state. The vibrational identifiers v are assigned to individual vibrational states as follows: $0 \rightarrow$ ground state, $1 \rightarrow \nu_{18} = 1$, $2 \rightarrow \nu_{18} = 2$, $3 \rightarrow \nu_{13} = 1$, $4 \rightarrow \nu_{18} = 3$, $5 \rightarrow (\nu_{18} = 1, \nu_{13} = 1)$, $6 \rightarrow \nu_{12} = 1$, $7 \rightarrow \nu_{17} = 1$, $8 \rightarrow \nu_{18} = 4$, $9 \rightarrow (\nu_{18} = 2, \nu_{13} = 1)$, and $10 \rightarrow \nu_{13} = 2$. The off-diagonal blocks are composed by the Coriolis and Fermi interaction Hamiltonians $\alpha H_{\text{Cor}}^{(v,v')}$ and $H_{\text{F}}^{(v,v')}$, respectively, and were used when clear evidence of the mutual interactions between two states v and v' was found. The leading terms of the α -type Coriolis Hamiltonian up to the second power in angular

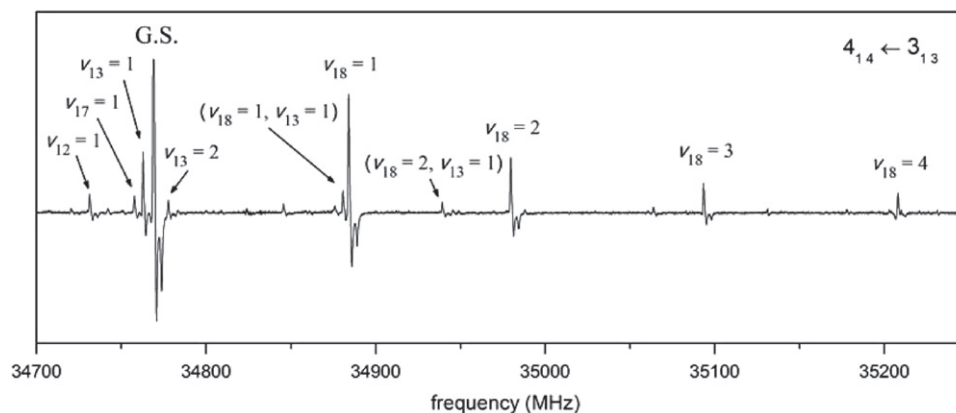


Figure 2. Stark modulated spectrum of the $J'_{K'_a K'_c} \leftarrow J''_{K''_a K''_c} = 4_{14} \leftarrow 3_{13}$ transition (modulation voltage 200 V) showing the assignments of the vibrational states below 700 cm^{-1} .

Table 3
Spectroscopic Constants of *Trans*-propenal for Each Vibrational State ν included in the Global 11-state Fit (*A*-reduction, I^L -representation)

OC ^b	Constant ^c	Unit	ν^a					
			0	1	2	3	4	5
100 $\nu\nu'$	<i>A</i>	MHz	47353.6999 (17) ^d	45782.9630 (50)	44374.617 (61)	48755.457 (49)	43101.272 (93)	46956.217 (86)
200 $\nu\nu'$	<i>B</i>	MHz	4659.499451 (93)	4666.24463 (33)	4672.9124 (10)	4659.3132 (10)	4679.4475 (17)	4665.4082 (17)
300 $\nu\nu'$	<i>C</i>	MHz	4242.689513 (86)	4259.62456 (32)	4276.62153 (90)	4238.35294 (96)	4293.6518 (14)	4255.7034 (11)
2 $\nu\nu'$	$-\Delta_J$	kHz	-1.042093 (30)	-1.087069 (83)	-1.13228 (17)	-1.02736 (16)	-1.18057 (18)	-1.06618 (13)
11 $\nu\nu'$	$-\Delta_{JK}$	kHz	8.79047 (56)	8.5734 (12)	8.2463 (68)	10.2970 (59)	8.3705 (97)	9.667 (10)
20 $\nu\nu'$	$-\Delta_K$	kHz	-360.260 (44)	64.74 (10)	327.99 (35)	-803.12 (23)	507.10 (41)	-149.07 (36)
401 $\nu\nu'$	$-\delta_J$	kHz	-0.120239 (11)	-0.119011 (66)	-0.11652 (15)	-0.11803 (15)	-0.11483 (15)	-0.116933 (68)
410 $\nu\nu'$	$-\delta_K$	kHz	-5.7747 (39)	0.769 (28)	6.258 (67)	-11.756 (68)	10.237 (63)	-2.335 (38)
3 $\nu\nu'$	Φ_J	mHz	0.3090 (39)	0.513 (13)	0.688 (35)	0.185 (33)	1.068 (33)	0.3090 ^e
12 $\nu\nu'$	Φ_{JK}	mHz	12.2 (17)	-101.1 (22)	-232 (11)	95 (11)	-74.7 (91)	-58.7 (84)
21 $\nu\nu'$	Φ_{KJ}	Hz	-0.5951 (64)	0.9430 (99)	2.460 (50)	-1.905 (41)	1.805 (41)	1.065 (42)
30 $\nu\nu'$	Φ_K	Hz	1.42 (25)	-217.87 (48)	-277.53 (71)	161.49 (49)	-299.60 (66)	-232.43 (82)
402 $\nu\nu'$	ϕ_J	mHz	0.0760 (17)	0.0858 (83)	-0.069 (21)	0.151 (23)	0.182 (19)	0.0760 ^e
411 $\nu\nu'$	ϕ_{JK}	mHz	7.99 (96)	60.7 (49)	93 (12)	-78 (11)	142 (11)	7.99 ^e
420 $\nu\nu'$	ϕ_K	Hz	2.63 (25)	-13.72 (33)	-31.5 (15)	16.7 (17)	-10.0 (12)	-6.8 (11)
$\nu\nu'$	ΔE	cm ⁻¹	0	157.883986 (22)	314.19009 (26)	323.05132 (25)	468.94645 (68)	482.82732 (68)
	<i>J</i> range ^f		0-77	2-74	2-70	3-73	2-71	3-70
	<i>K_a</i> range ^f		0-24	0-22	0-20	0-21	0-17	0-15
	<i>N</i> _{lines} / <i>N</i> _{ex} ^g		1983/1	1728/23	936/0	947/1	977/10	811/12
OC ^b	Constant ^c	Unit	6	7	8	9	10	
100 $\nu\nu'$	<i>A</i>	MHz	47416.470 (69)	47190.191 (58)	41959.25 (94)	45351.42 (89)	50229.95 (13)	...
200 $\nu\nu'$	<i>B</i>	MHz	4656.00325 (58)	4653.5032 (10)	4686.1597 (97)	4671.2440 (83)	4659.2597 (25)	...
300 $\nu\nu'$	<i>C</i>	MHz	4237.96030 (46)	4242.15421 (76)	4310.8450 (53)	4273.1641 (46)	4234.0391 (24)	...
2 $\nu\nu'$	$-\Delta_J$	kHz	-1.04737 (16)	-1.04841 (19)	-1.22103 (33)	-1.09837 (54)	-1.02430 (53)	...
11 $\nu\nu'$	$-\Delta_{JK}$	kHz	9.074 (12)	9.410 (13)	7.935 (28)	9.036 (23)	12.082 (18)	...
20 $\nu\nu'$	$-\Delta_K$	kHz	-357.36 (47)	-368.38 (15)	584.0 (46)	279.9 (41)	-1365.53 (91)	...
401 $\nu\nu'$	$-\delta_J$	kHz	-0.119715 (39)	-0.11940 (16)	-0.10875 (21)	-0.11748 (59)	-0.11000 (53)	...
410 $\nu\nu'$	$-\delta_K$	kHz	-6.242 (53)	-5.413 (59)	-13.143 (90)	-10.39 (20)	20.47 (19)	...
3 $\nu\nu'$	Φ_J	mHz	0.332 (26)	0.412 (32)	1.488 (36)	-0.75 (13)	-1.10 (13)	...
12 $\nu\nu'$	Φ_{JK}	mHz	82.1 (53)	8.3 (18)	-192 (28)	-955 (20)	1022 (35)	...
21 $\nu\nu'$	Φ_{KJ}	Hz	-0.5951 ^e	-0.339 (16)	3.90 (15)	5.49 (14)	-6.34 (10)	...
30 $\nu\nu'$	Φ_K	Hz	5.5 (15)	-25.65 (36)	-223.4 (95)	-409.5 (77)	426.5 (18)	...
402 $\nu\nu'$	ϕ_J	mHz	0.0760 ^e	0.087 (20)	-0.531 (37)	-1.09 (11)	0.79 (10)	...
411 $\nu\nu'$	ϕ_{JK}	mHz	18.5 (93)	50 (11)	7.99 ^e	-206 (56)	-617 (52)	...
420 $\nu\nu'$	ϕ_K	Hz	13.14 (75)	2.63 ^e	-23.2 (37)	-130.8 (32)	145.9 (49)	...
$\nu\nu'$	ΔE	cm ⁻¹	564.340326 (23)	593.079293 (15)	621.8530 (40)	641.0928 (41)	647.83644 (57)	...
	<i>J</i> range ^f	...	3-70	3-69	2-70	3-67	3-66	...
	<i>K_a</i> range ^f	...	0-15	0-17	0-15	0-15	0-17	...
	<i>N</i> _{lines} / <i>N</i> _{ex} ^g	...	798/7	649/20	602/42	505/34	463/7	...

Note.

^a The assignment of the vibrational states to ν is as following: 0 \rightarrow ground state, 1 $\rightarrow \nu_{18} = 1$, 2 $\rightarrow \nu_{18} = 2$, 3 $\rightarrow \nu_{13} = 1$, 4 $\rightarrow \nu_{18} = 3$, 5 $\rightarrow (\nu_{18} = 1, \nu_{13} = 1)$, 6 $\rightarrow \nu_{12} = 1$, 7 $\rightarrow \nu_{17} = 1$, 8 $\rightarrow \nu_{18} = 4$, 9 $\rightarrow (\nu_{18} = 2, \nu_{13} = 1)$, and 10 $\rightarrow \nu_{13} = 2$.

^b SPFIT/SPCAT operator code. These operators are each within a defined state ν where $\nu = \nu' = 0, 1, \dots, 10$.

^c Common constant symbol.

^d The numbers in parentheses are 1σ uncertainties in the units of the last decimal digit.

^e Fixed to the ground state value.

^f Quantum number range corresponding to the millimeter and submillimeter data.

^g Number of distinct frequency fitted lines/number of excluded lines corresponding to the pure rotational data based on the $9u$ fitting criterion of the SPFIT program where u is the uncertainty of the measured frequency.

momentum are (Prevalov & Tyuterev 1982)

$$\alpha H_{\text{Cor}}^{(\nu, \nu')} = iG_\alpha J_\alpha + F_{\beta\gamma} (J_\beta J_\gamma + J_\gamma J_\beta) \quad (2)$$

where G_α and $F_{\beta\gamma}$ are the Coriolis coupling constants α, β, γ are the permutations of a, b, c . The Fermi interaction

Hamiltonian up to the second power in angular momentum is given as (Prevalov & Tyuterev 1982)

$$H_{\text{F}}^{(\nu, \nu')} = W + W_J J^2 + W_K J_a^2 + W_\pm (J_b^2 - J_c^2) \quad (3)$$

Table 4
Coriolis and Fermi Coupling Constants for Interacting States ($v \leftrightarrow v'$) of *Trans*-propenal Obtained from the Global 11-state Fit (\mathcal{F} -representation)

OC ^b	Constant ^c	Unit	$(v \leftrightarrow v')^a$					
			(0 \leftrightarrow 1)	(1 \leftrightarrow 2)	(6 \leftrightarrow 7)	(7 \leftrightarrow 8)	(7 \leftrightarrow 9)	(7 \leftrightarrow 10)
2000 $v v'$	G_a	MHz	11272.5 (21) ^d	131.3 (20)	-413 (15)	...
2001 $v v'$	G_a^J	MHz	-0.02270 (44)
2100 $v v'$	F_{bc}	MHz	1.0621 (30)
4000 $v v'$	G_b	MHz	1132.26 (13)	43.37 (70)	-69.9 (69)	...
4001 $v v'$	G_b^J	kHz	0.0239 (88)
4010 $v v'$	G_b^K	MHz	-0.1287 (14)
4100 $v v'$	F_{ac}	MHz	5.48 (26)	...
4200 $v v'$...	kHz	5.606 (49)
4210 $v v'$...	kHz	...	0.02467 (19)

OC ^b	Constant ^c	Unit	$(v \leftrightarrow v')$					
			(2 \leftrightarrow 3)	(4 \leftrightarrow 5)	(6 \leftrightarrow 8)	(8 \leftrightarrow 9)	(8 \leftrightarrow 10)	(9 \leftrightarrow 10)
6000 $v v'$	G_c	MHz	-345.488 (34)	550.203 (35)	77.54 (10)	650.24 (30)	-98.8 (13)	534.61 (40)
6001 $v v'$	G_c^J	kHz	0.388 (13)
6100 $v v'$	F_{ab}	MHz	-1.6356 (22)	2.2549 (25)	3.432 (22)
6200 $v v'$...	kHz	-0.571 (10)	0.9216 (34)	3.997 (73)	0.210 (23)
$v v'$	W	MHz	81372 (13)	-134480 (32)	...	168296 (202)	...	116018 (15)
1 $v v'$	W_J	MHz	-0.2174 (16)	0.5528 (30)	-0.2685 (27)
10 $v v'$	W_K	MHz	-52.12 (15)	56.78 (18)	...	-111.5 (28)	...	-73.86 (29)
11 $v v'$	W_{JK}	kHz	-1.015 (29)	0.993 (28)
400 $v v'$	W_{\pm}	MHz	-0.0790 (57)
410 $v v'$	W_{\pm}^K	kHz	...	0.308 (28)
1200 $v v'$...	kHz	0.797 (47)	...

Note.

^a The assignment of the vibrational states to v is as following: 0 \rightarrow ground state, 1 $\rightarrow v_{18} = 1$, 2 $\rightarrow v_{18} = 2$, 3 $\rightarrow v_{13} = 1$, 4 $\rightarrow v_{18} = 3$, 5 $\rightarrow (v_{18} = 1, v_{13} = 1)$, 6 $\rightarrow v_{12} = 1$, 7 $\rightarrow v_{17} = 1$, 8 $\rightarrow v_{18} = 4$, 9 $\rightarrow (v_{18} = 2, v_{13} = 1)$, and 10 $\rightarrow v_{13} = 2$.

^b SPFIT/SPCAT operator code. These operators each connect defined vibrational states v and v' where $v \neq v'$ and $v, v' = 0, 1, \dots, 10$.

^c Common constant symbol.

^d The numbers in parentheses are 1σ uncertainties in the units of the last decimal digit.

Table 5
Predicted Transition Frequencies of the *Trans*- and *Cis*-propenal Ground States and Ten Excited Vibrational States of *Trans*-propenal

Species	Transition ^a								ν_{calc}^b (MHz)	$u(\nu_{\text{calc}})^c$ (MHz)	$S\mu^2d$ (D ²)	E^e (cm ⁻¹)	E^{f} (cm ⁻¹)
	J'	K'_a	K'_c	v'	J''	K''_a	K''_c	v''					
<i>Trans</i>	10	2	8	3	9	2	7	3	89423.789	0.005	733.300	346.055	343.072
<i>Trans</i>	10	5	6	2	9	5	5	2	89431.879	0.010	574.612	363.332	360.349
<i>Trans</i>	10	2	8	0	9	2	7	0	89436.162	0.001	733.476	22.098	19.115
<i>Cis</i>	8	6	2	0	7	6	1	0	89445.730	0.002	101.415	34.124	31.140
<i>Cis</i>	21	4	17	0	21	3	18	0	89523.928	0.025	182.948	97.469	94.483
<i>Cis</i>	8	5	4	0	7	5	3	0	89527.729	0.003	141.241	27.803	24.817

Note. Only transitions with predicted uncertainties $u(\nu_{\text{calc}}) \leq 1$ MHz are included.

^a Upper and lower state quantum numbers are indicated by ' and '', respectively. The assignment of the individual vibrational states to v is as following: 0 \rightarrow ground state, 1 $\rightarrow v_{18} = 1$, 2 $\rightarrow v_{18} = 2$, 3 $\rightarrow v_{13} = 1$, 4 $\rightarrow v_{18} = 3$, 5 $\rightarrow (v_{18} = 1, v_{13} = 1)$, 6 $\rightarrow v_{12} = 1$, 7 $\rightarrow v_{17} = 1$, 8 $\rightarrow v_{18} = 4$, 9 $\rightarrow (v_{18} = 2, v_{13} = 1)$, and 10 $\rightarrow v_{13} = 2$.

^b Predicted frequency.

^c 1σ uncertainty of the predicted frequency.

^d Line strength S multiplied by the square of the dipole moment component. Experimentally available values of the dipole moment of $|\mu_a| = 3.052$ D and $|\mu_b| = 0.630$ D for *trans*-propenal and $|\mu_b| = 2.010$ D and $|\mu_b| = 1.573$ D (Blom et al. 1984) for *cis*-propenal were used in the calculation. Dipole moment components for *trans*-propenal excited vibrational states were approximated by corresponding ground state values.

^e Upper level energy.

^f Lower level energy.

(This table is available in its entirety in machine-readable form.)

where W , W_J , W_K , and W_{\pm} are the Fermi coupling constants. Despite the huge convergence problems, a stable fit was

eventually achieved by finally selecting 211 adjusted and 7 fixed parameters leading to root mean square deviation of

168 kHz. Analysis of many interstate perturbations allowed to derive precise values of vibrational energies for all the excited vibrational states and together with the rotational and centrifugal distortion constants are assembled in Table 3. Determinable Coriolis and Fermi coupling constants are listed in Table 4. Choice of the Coriolis and Fermi coupling constants related to higher powers of angular momentum operators, than those presented in Equations (2) and (3), has been established empirically during the fitting procedure. Those producing a significant improvement of the fit were retained. Some of these constants, however, do not have generally known symbols. SPFIT/SPCAT operator codes are thus provided in Tables 3 and 4 to be able to derive the corresponding operator form. In the basis of J^2 , J_a^2 , and J_{\pm} , where $J_{\pm} = J_b \pm iJ_c$, definition of such operators can be found in Butler et al. (2003) or Pearson et al. (2008). Spectroscopic constants reported in Tables 3 and 4 can be considered as effective parameters that reproduce precisely the rotational spectrum *trans*-propenal in the ground and ten excited vibrational states.

Since the intensities are prerequisite for a correct molecular identification in the ISM, the spectroscopic constants from Tables 1–4 were used to predict the transition frequencies and line strengths of both isomers studied in this work in the frequency region through 760 GHz. The predicted transition frequencies are gathered in Table 5 along with the rotational quantum numbers, estimated uncertainties, intensities in terms of line strengths multiplied by the square of the corresponding dipole moment component, and energies of the lower and upper energy levels.

To sum up, present laboratory measurements and complete analysis of the propenal millimeter and submillimeter spectra have allowed to determine new sets of the spectroscopic constants and, using the available values of the dipole moment components, it was possible to predict the transition frequencies and intensities of many additional lines through 760 GHz. Rotational transitions of propenal can now be searched for over a wide frequency range toward appropriate interstellar sources.

This research has been supported by the “Ministerio de Ciencia e Innovación” (grant numbers CTQ 2013-40717 P, CTQ 2010-19008 and CONSOLIDER-Ingenio program “ASTROMOL,” CSD 2009-00038) and Junta de Castilla y

León (Grants VA070A08 and VA175U13). C.B. wishes to thank the Ministerio de Ciencia e Innovación for an FPI grant (BES 2011-047695).

REFERENCES

- Beltrán, M. T., Codella, C., Viti, S., Neri, R., & Cesaroni, R. 2009, *ApJL*, **690**, L93
- Bermúdez, C., Peña, I., Cabezas, C., Daly, A. M., & Alonso, J. L. 2013, *ChemPhysChem*, **14**, 893
- Blom, C. E., & Bauder, A. 1982, *CPL*, **88**, 55
- Blom, C. E., Grassi, G., & Bauder, A. J. 1984, *JChS*, **106**, 7427
- Butler, R. A. H., Petkie, D. T., Helminger, P., & de Lucia, F. C. 2003, *JMoSp*, **220**, 150
- Cherniak, E. A., & Costain, C. C. 1966, *JChPh*, **45**, 104
- Cole, A. R. H., & Green, A. A. 1973, *JMoSp*, **48**, 232
- Daly, A. M., Bermúdez, C., López, A., et al. 2013, *ApJ*, **768**, 81
- Daly, A. M., Kolesníková, L., Mata, S., & Alonso, J. L. 2014, *JMoSp*, **306**, 11
- Dickens, J. E., Irvine, W. M., & Nummelin, A. 2001, *AcSpA*, **57**, 643
- Halfen, D. T., Apponi, A. J., Woolf, N., Polt, R., & Ziurys, L. M. 2006, *ApJ*, **639**, 237
- Fine, J., Goldstein, J. H., & Simmons, J. W. 1955, *JChPh*, **23**, 601
- Hollis, J. M., Jewell, P. R., Lovas, F. J., Remijan, A., & Mollendal, H. 2004, *ApJL*, **610**, L21
- Hollis, J. M., Lovas, F. J., & Jewell, P. R. 2000, *ApJL*, **540**, L107
- Ikeda, M., Ohishi, M., Nummelin, A., et al. 2001, *ApJ*, **560**, 792
- Irvine, W. M., Brown, R. D., Cragg, D. M., et al. 1988, *ApJL*, **335**, L89
- Jørgensen, J. K., Favre, C., Bisschop, S. E., et al. 2012, *ApJL*, **757**, L4
- Kisiel, Z., Pszczolkowski, L., Drouin, B., et al. 2012, *JMoSp*, **280**, 134
- Kisiel, Z., Pszczolkowski, L., Medvedev, I. R., et al. 2005, *JMoSp*, **233**, 231
- Loomis, F. W., & Wood, R. W. 1928, *PhRv*, **32**, 223
- López, A., Tercero, B., Kisiel, Z., et al. 2014, *A&A*, **572**, A44
- McKellar, A. R. W., & Appadoo, D. R. T. 2008, *JMoSp*, **250**, 106
- McKellar, A. R. W., Tokaryk, D. W., Xu, L. H., Appadoo, D. R. T., & May, T. 2007, *JMoSp*, **242**, 31
- Moldoveanu, S. 2010, *Pyrolysis of Organic Molecules: Applications to Health and Environmental Issues*, Vol. 28 (Amsterdam: Elsevier)
- Pickett, H. M. 1991, *JMoSp*, **148**, 371
- Pearson, J. C., Brauer, C. S., & Drouin, B. J. 2008, *JMoSp*, **251**, 394
- Prevalov, V. I., & Tyuterev, V. G. 1982, *JMoSp*, **96**, 56
- Requena-Torres, M. A., Martín-Pindado, J., Martín, S., & Morris, M. R. 2008, *ApJ*, **672**, 352
- Turner, B. E. 1991, *ApJS*, **76**, 617
- Snyder, L. E., Buhl, D., Zuckerman, B., & Palmer, P. 1969, *PhRv*, **22**, 679
- van Trump, J. E., & Miller, S. L. 1972, *Sci*, **178**, 859
- Wagner, R., Fine, J., Simmons, J. W., & Goldstein, J. H. 1957, *JChPh*, **26**, 634
- Watson, J. K. G. 1977, *Vibrational Spectra and Structure*, Vol. 6 (Amsterdam: Elsevier)
- Winniewisser, M., Winniewisser, G., Honda, T., & Hirota, E. 1975, *ZNatA*, **30A**, 1001
- Xu, L. H., Jiang, X., Shi, H., et al. 2011, *JMoSp*, **268**, 136